

RESEARCH LETTER

10.1002/2017GL073383

Special Section:

Early Results: Juno at Jupiter

Key Points:

- Jupiter's North Equatorial Belt expanded northward in 2015/2016 as part of its 3–5 year activity cycle
- The expanded sector warmed, removing light-colored aerosols to reveal darker colors at depth
- Significant thermal waves were identified in the troposphere and stratosphere at the time of the expansion

Supporting Information:

- Supporting Information S1

Correspondence to:

L. N. Fletcher,
leigh.fletcher@leicester.ac.uk

Citation:

Fletcher, L. N., et al. (2017), Jupiter's North Equatorial Belt expansion and thermal wave activity ahead of Juno's arrival, *Geophys. Res. Lett.*, 44, 7140–7148, doi:10.1002/2017GL073383.












Received 9 MAR 2017

Accepted 12 APR 2017

Accepted article online 25 MAY 2017

Published online 31 JUL 2017

Jupiter's North Equatorial Belt expansion and thermal wave activity ahead of Juno's arrival

L. N. Fletcher¹ , G. S. Orton² , J. A. Sinclair² , P. Donnelly¹, H. Melin¹ , J. H. Rogers³, T. K. Greathouse⁴ , Y. Kasaba⁵ , T. Fujiyoshi⁶, T. M. Sato⁷ , J. Fernandes⁸, P. G. J. Irwin⁹ , R. S. Giles⁹, A. A. Simon¹⁰ , M. H. Wong¹¹ , and M. Vedovato¹² 
¹Department of Physics and Astronomy, University of Leicester, Leicester, UK, ²Jet Propulsion Laboratory, California Institute of Technology, Pasadena, California, USA, ³British Astronomical Association, London, UK, ⁴Southwest Research Institute, San Antonio, Texas, USA, ⁵Department of Geophysics, Tohoku University, Sendai, Japan, ⁶Subaru Telescope, National Astronomical Observatory of Japan, National Institutes of Natural Sciences, Hilo, Hawaii, USA, ⁷Institute of Space and Astronautical Science, Japan Aerospace Exploration Agency, Sagami-hara, Japan, ⁸Department of Physics and Astronomy, California State University, Long Beach, California, USA, ⁹Atmospheric, Oceanic and Planetary Physics, Department of Physics, University of Oxford, Oxford, UK, ¹⁰Solar System Exploration Division (690), NASA Goddard Space Flight Center, Greenbelt, Maryland, USA, ¹¹Astronomy Department, University of California, Berkeley, California, USA, ¹²JUPOS Team, Unione Astrofili Italiani, Rome, Italy

Abstract The dark colors of Jupiter's North Equatorial Belt (NEB, 7–17°N) appeared to expand northward into the neighboring zone in 2015, consistent with a 3–5 year cycle. Inversions of thermal-IR imaging from the Very Large Telescope revealed a moderate warming and reduction of aerosol opacity at the cloud tops at 17–20°N, suggesting subsidence and drying in the expanded sector. Two new thermal waves were identified during this period: (i) an upper tropospheric thermal wave (wave number 16–17, amplitude 2.5 K at 170 mbar) in the mid-NEB that was anticorrelated with haze reflectivity; and (ii) a stratospheric wave (wave number 13–14, amplitude 7.3 K at 5 mbar) at 20–30°N. Both were quasi-stationary, confined to regions of eastward zonal flow, and are morphologically similar to waves observed during previous expansion events.

Plain Language Summary A campaign of Earth-based support imaging for NASA's Juno mission identified several interesting atmospheric phenomena at work in Jupiter's northern hemisphere. The prominent dark brown belt north of the equator expanded northward, potentially spawning wave activity throughout the troposphere and stratosphere. Unlike previous cyclic events on Jupiter (these expansions occur once every 3–5 years), the 2015/2016 expansion stalled and did not reach completion, but the waves were evident throughout 2016 ahead of Juno's arrival in orbit around Jupiter. Such Earth-based supporting observations help set the environmental context for Juno's close-up observations of the giant planet.

1. Introduction

Jupiter's banded appearance can exhibit dramatic global-scale variability, with the dark belts expanding, contracting, and sometimes whitening for many months at a time [e.g., Rogers, 1995; Sánchez-Lavega and Gomez, 1996; Fletcher et al., 2017, and references therein]. These are the visible manifestations of thermal, chemical, and aerosol changes throughout Jupiter's upper troposphere, which can be best diagnosed at thermal-infrared wavelengths. As NASA's Juno spacecraft lacks instrumentation at these wavelengths, a campaign of Earth-based observations is underway to characterize Jupiter's thermal structure. Here we report on the identification of a poleward expansion of Jupiter's North Equatorial Belt (NEB) and significant thermal wave activity in observations acquired in the months before Juno's arrival.

The NEB is a broad, brown, cyclonic belt typically residing between eastward and westward jets at 6.8°N and 17.1°N, respectively (all latitudes are planetographic). Visible observations have shown that the northern edge exhibits regular northward expansion events [Rogers, 1995], causing a decrease in reflectivity (darkening) of the southern edge (17–21°N) of the white North Tropical Zone (NTrZ) with a 3 to 5 year period since 1987 [Rogers, 2017]. Text S1 and Figure S1 in the supporting information show details of seven NEB expansion

events recorded since 1987. These events either start from a single “bulge” of dark material encroaching into the NTrZ or occur simultaneously at multiple longitudes, infilling and spreading over all longitudes over ~ 5 –7 months (Text S1). The newly darkened NTrZ then whitens over 1–3 years, such that the edge of the brown belt appears to recede southward to the normal 7 – 17°N range. Infrared observations of the 2009–2011 event demonstrated that the darkening of the NTrZ corresponded to a removal of aerosol opacity at $5\text{ }\mu\text{m}$ [Fletcher *et al.*, 2017]. The cyclic nature of the NEB activity suggested that a new expansion phase would occur in 2015–2016, which we characterize here.

Jupiter's NEB and NTrZ also host wave phenomena. A long-lived pattern of cloud-free “hot spots” and associated plumes has been observed on the NEB southern edge [Choi *et al.*, 2013, and references therein], manifesting an equatorially trapped Rossby wave [Allison, 1990; Showman and Dowling, 2000; Friedson, 2005]. The interior of the NEB is characterized by upper tropospheric thermal wave activity [e.g., Magalhaes *et al.*, 1990; Orton *et al.*, 1994; Rogers *et al.*, 2004; Li *et al.*, 2006; Fisher *et al.*, 2016]. Stratospheric waves in the 20 – 30°N region were also reported [Orton *et al.*, 1991; Fletcher *et al.*, 2016]. A chronology of these previous wave detections is presented in Text S2.

2. Earth-Based Thermal Observations

Narrowband 8 – $25\text{ }\mu\text{m}$ thermal imaging of Jupiter (Table S1) was acquired in January 2016 by the COMICS instrument [Katata *et al.*, 2000] on the Subaru Telescope and between February and August 2016 by the VISIR instrument [Lagage *et al.*, 2004] on ESO's Very Large Telescope (VLT, Figure S2). These 8 m primary mirrors provide diffraction-limited spatial resolutions of 0.25 – $0.80''$ (700 – 2300 km at Jovian opposition). Full details of both instruments and the strategy for Jupiter observations are given by Fletcher *et al.* [2017]. Fletcher *et al.* [2009] describe image reduction procedures: images were despiked and cleaned for bad pixels, geometrically registered by fitting the planetary limb, cylindrically reprojected and calibrated via comparison to Cassini Composite Infrared Spectrometer observations. This time series was supplemented in January and May 2016 by spectroscopic mapping at 17.1 and $8.0\text{ }\mu\text{m}$ (at spectral resolutions of 5800 and 12,400, respectively) using the TEXES instrument on NASA's Infrared Telescope Facility (IRTF) [Lacy *et al.*, 2002], albeit at lower diffraction-limited spatial resolution from IRTF's smaller 3 m primary mirror. Fletcher *et al.* [2016] give full details of the spectral scanning technique. Images and scans acquired over two or more consecutive nights were combined to create near-global maps of Jupiter.

Radiance maps in eight VISIR filters were stacked to form spectral cubes for inversion using an optimal-estimation retrieval algorithm [Irwin *et al.*, 2008]. This allows estimates of the spatial variability of stratospheric temperatures near 5 mbar from CH_4 emission at $7.9\text{ }\mu\text{m}$, 100 – 600 mbar tropospheric temperatures from 13 to $24\text{ }\mu\text{m}$ observations of the H_2 and He collision-induced continuum, and tropospheric aerosols near 600 – 800 mbar from 8 to $12\text{ }\mu\text{m}$ observations of NH_3 absorption bands. With only eight photometric points defining each spectrum, the inversion suffers from limited vertical resolution and some degeneracies between retrieved parameters (particularly for high pressures). Details of the inversion methodology and sources of spectral line data are given by Fletcher *et al.* [2009].

3. Results and Discussion

3.1. Chronology of the 2015–2016 NEB Expansion

The evolution of the 2015–2016 NEB expansion event has been characterized in both visible-light observations from amateur observers (Text S3 and Figures S3 and S4 in the supporting information) and in the thermal-infrared (Figure 1). This can be compared to Hubble WFC3 imaging in February 2016 (see also Figure S5). The exact starting date of the expansion is uncertain, as no identifiable plumes are involved. Bulges of dark NEB colors gradually appeared near 16 – 18°N , west of the prominent White Spot Z (WSZ) near 19°N , 283°W , an oval which has persisted since 1997 [Rogers, 2013]. These dark bulges were present as early as October 2014 (Text S3) and are visible in Hubble WFC3 imaging in January 2015 (Figure S5) [Simon *et al.*, 2015], but appeared ephemerally between March and June 2015 (Figure S3). By October 2015, the expanded sector spanned 80° of longitude between 320° and 40°W . This sector expanded east, reaching the WSZ, and west to a dark cyclone-anticyclone pair near 50 – 60°W , through January 2016 by infilling gaps between NEB bulges, occupying $\sim 120^\circ$ of longitude at the start of 2016 (Figure 1).

Figure 1 shows that the northern edge of the expanded NEB was at a higher latitude (20°N) than elsewhere (17°N), having replaced the white appearance of the NTrZ with darker colors. The NEB appears bright at

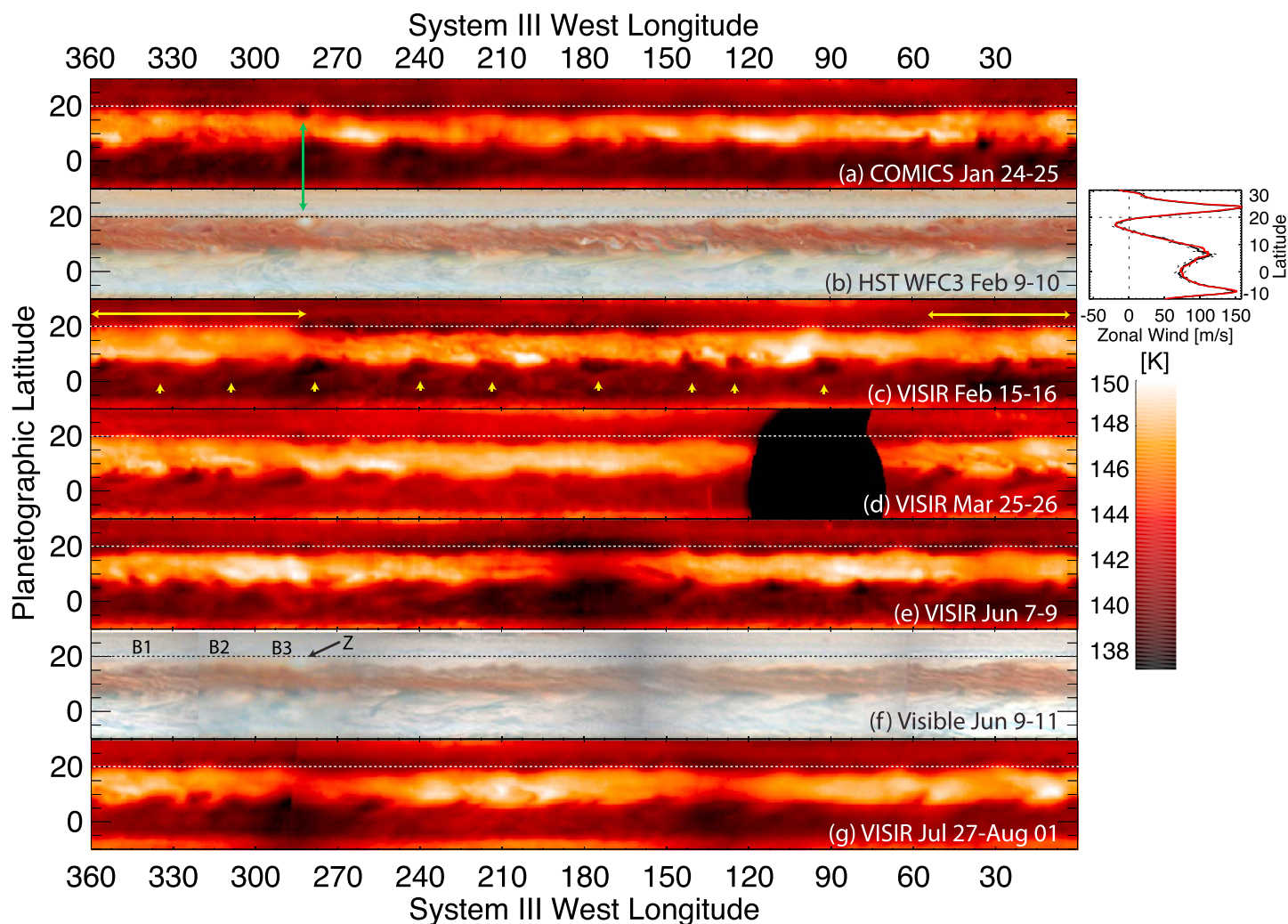


Figure 1. Time series of 8.6 μm brightness temperature maps, January–August 2016. Yellow arrows denote the expanded sector; barges B1–B3 are labeled in Figure 1f. Green arrows in Figure 1b show White Spot Z. The visible-light maps in Figure 1b were provided by Hubble WFC3 in February (see Figure S5), and by amateur observers in Figure 1f in June. Hot spots and plumes (denoted by small yellow arrows) can be seen as bright and dark features on the southern edge of the NEB, respectively (Text S4). Horizontal lines at 20°N in each panel show the maximum extent of the expanded sector. Cloud top zonal winds from Hubble imaging in February 2016 (black) and January 2015 (red) are shown next to Figure 1b, indicating no change in either the jet location or speed [Tollefson *et al.*, 2017].

8.6 μm due to a combination of warmer temperatures and low aerosol opacity, and the expanded sector of the NEB appears notably brighter than the undisturbed NTRZ (50–270°W), consistent with the enhanced 5 μm brightness of the 2009–2010 expansion event [Fletcher *et al.*, 2017].

Previous NEB expansions have encircled the entire globe (Text S1), but the 2016 expansion only reached a maximum of $\sim 145^\circ$ longitude by March and then regressed from both ends, rerevealing the NEB dark bulges. VISIR images in March 2016 suggested that the northern edge of the expanded NEB (17–20°N) was dimming at 8.6 μm , reestablishing aerosol opacity over the NTRZ. Visible-light images (Figure S4) show a continued regression in April and May, and by June (Figures 1e and 1f) the expanded sector had returned to normal, although some faint orange coloration could still be seen in the previously expanded sectors. The 8.6 μm dark NTRZ could be seen to extend around the planet once more. Thus, neither visible-light images from JunoCAM [Orton *et al.*, 2017] nor 5 μm images from Juno/JIRAM [Adriani *et al.*, 2016] showed any signs of the expansion at the first Juno perijove on 27 August 2016. The exception is the presence of four newly formed dark brown “barges” near 16–17°N, B1–B4 (Figure 1f), that formed in the NEB during the expansion phase (Text S3). After the recession of the expansion, these barges remained visible on the northern edge of the “normal” NEB.

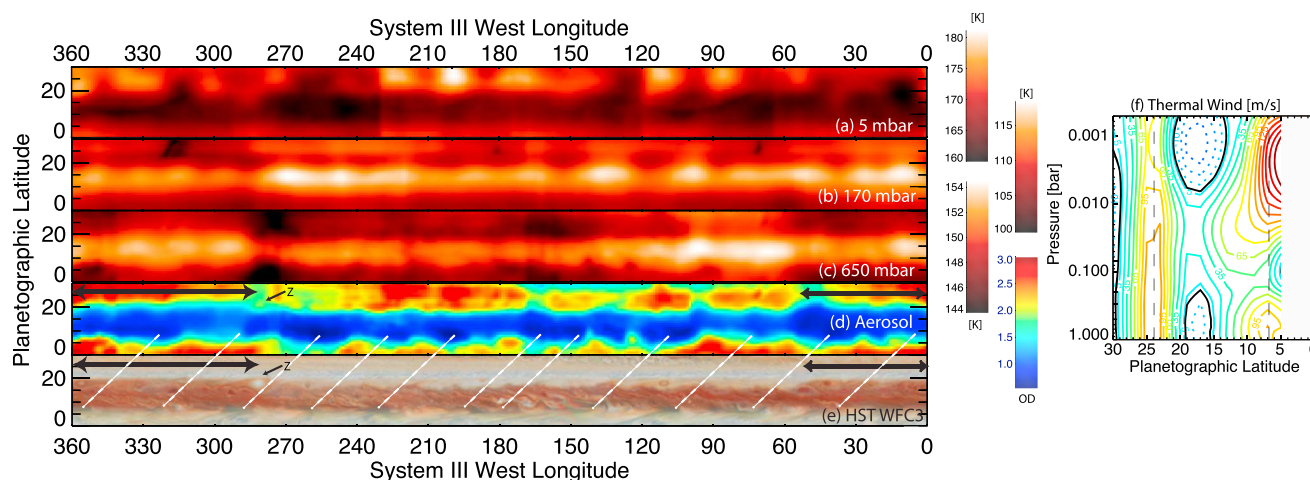


Figure 2. Retrieved maps of temperature and aerosol opacity using VLT/VISIR observations on 15–16 February 2016. Shown are temperatures at (a) 5, (b) 170, and (c) 650 mbar with uncertainties (Figure S7) of ± 5 , ± 3 , and ± 3 K, respectively. (d) The cumulative aerosol optical depth at $10 \mu\text{m}$, integrated to the 1 bar level, assumed to comprise NH_3 ices in a ~ 600 – 800 mbar cloud layer. Only aerosol optical depth is varied, other aerosol properties (absorption cross section, single-scattering albedo, and vertical structure) are assumed to be invariant. (e) The Hubble WFC3 map from 9 to 10 February (Figure 1b), with white dashed lines showing the cloud-free hot spot locations in Figures 2d and 2e. The expanded sector of the NEB is indicated by black horizontal arrows in Figures 2d and 2e. Cold, cloudy plumes lie immediately east of the hot spots. Zonal winds are shown in Figure 2f, estimated from TEXES observations in December 2014 [Fletcher *et al.*, 2016]. Dashed vertical lines show the locations of the NTBs and NEBs eastward jets, solid black contours indicate $u = 0$ m/s, and dashed contours indicate westward winds.

3.2. Thermal Changes During a NEB Expansion

What physical conditions are associated with the NEB expansion? Either (i) a low-albedo brown aerosol forms over the NTrZ, or (ii) some dynamical process removes white aerosols from the NTrZ so that its coloration matches the NEB. Hypothesis (ii) is akin to aerosol clearing events following a whitening of the South Equatorial Belt (SEB) [Fletcher *et al.*, 2011], and was suggested for the 2009–2011 expansion event [Fletcher *et al.*, 2017]. Maps at eight wavelengths (7.9, 8.6, 10.7, 12.3, 13.0, 17.6, 18.7, and $19.5 \mu\text{m}$) acquired over two nights (15–16 February) were combined to retrieve temperatures and aerosols in Figure 2. Absolute values are subject to large uncertainties resulting from the low information content of the eight-point spectra (see Figure S6), but relative contrasts are robust [Fletcher *et al.*, 2009]. Temperatures are shown at representative pressure levels in the stratosphere (5 mbar), upper troposphere (170 mbar), and near the cloud tops (650 mbar). The vertical structure of the zonal winds is also shown [Fletcher *et al.*, 2016].

The broad cool NTrZ at 19 – 24°N shows no evidence for thermal changes associated with the expanded NEB sector in the upper troposphere (100–500 mbar, Figure 2b). However, temperatures at 650 mbar (Figure 2c) suggest a 3–4 K warming in a diffuse warm area over the expanded sector at cloud top, coupled with a fall in the tropospheric aerosol opacity from ~ 2.8 (representative of the nonexpanded sectors) to ~ 1.5 for the expanded sector (Figure 2d). While still not as aerosol-free as most of the NEB (opacities < 1.0), this reduction of opacity, coupled with the moderate rise in temperature, suggests evaporative removal of the NTrZ white aerosols to reveal deeper red-brown chromophores, supporting hypothesis (ii). We caution the reader that temperature and aerosol changes are degenerate. Nevertheless, Hubble WFC3 observations at 890 nm (Figures 3d and S5), sensing upper tropospheric aerosols, confirm a lower reflectivity over the expanded sector, consistent with the removal of white NTrZ aerosols.

This association between tropospheric warmth and aerosol clearing is similar to that observed during the revival of Jupiter's SEB in 2011 [Fletcher *et al.*, 2017], where large-scale subsiding air masses removed aerosols in the regions surrounding convective plumes. However, no such localized vigorous plumes were associated with the NEB expansion. Vertical motions causing the NTrZ aerosol clearing could be related to the wave causing the ephemeral bulges on the northern edge of the NEB, but high-resolution wind measurements of any jet meanderings are not available (particularly regarding interaction between WSZ and the NEBn jet). Zonal winds derived from Hubble observations in January 2015 and February 2016 (Figure 1b) show no evidence for changes associated with the expansion [Tollefson *et al.*, 2017].

3.3. Upper Tropospheric NEB Wave

Although the NEB expansion had regressed completely by Juno's arrival, thermal waves identified in the 2016 data were still active. Figure 2b shows a wave pattern in the mid-NEB in the upper troposphere ($p < 500$ mbar), similar to that observed by previous studies [e.g., Magalhaes *et al.*, 1990; Orton *et al.*, 1994; Deming *et al.*, 1997; Li *et al.*, 2006; Fisher *et al.*, 2016]. The warm crests have a central latitude of $13\text{--}15^\circ\text{N}$, and the wave pattern is latitudinally confined to the bright belt at $10\text{--}17^\circ\text{N}$ ($\pm 1^\circ$). We measure temperature excursions of $1.5\text{--}4.0$ K with a mean amplitude of 2.5 K at 170 mbar (Figures 2, S7, and S8). The wave dominates the appearance of the upper troposphere and extends around the whole planet with a wave number $N \approx 16\text{--}17$ in January–February 2016, including nonexpanded NEB sectors. This equates to a horizontal wavelength of $25,700\text{--}27,400$ km, making the mid-NEB wave distinct from the plume/hot spot wave on the NEBs, which has $N \sim 12$ during this period (Text S4). The mid-NEB wave has no obvious counterpart in the main cloud deck. It is not detected in the stratosphere, consistent with observations in 2000 [Li *et al.*, 2006].

Figure 3 shows a time series of the tropospheric wave in $17.6\text{ }\mu\text{m}$ brightness temperatures (sensing ~ 150 mbar) from Subaru, VLT, and IRTF observations. Contrasts in the wave pattern appear to vary, but this could simply result from different observing conditions on different nights. We were unable to determine the phase speed of the wave from the thermal-IR data alone, as the gap between observations was too large, given the intrinsic variability of the wave pattern. However, inspection of near-infrared reflectivity observations in strong CH_4 bands, 890 nm from Hubble WFC3 and $2.16\text{ }\mu\text{m}$ observations from the NASA/IRTF SpeX instrument (Figure S9), taken between the COMICS observation on 24–25 January and the VISIR observation on 15–16 February, reveal a very similar wave pattern in the upper tropospheric aerosols. Figure 3 demonstrates that mid-NEB temperatures are anticorrelated with aerosol reflectivity due to either (i) aerosol evaporation or (ii) aerosol subsidence to deeper levels in the warm peaks of the mid-NEB wave. Such a correlation was previously shown for the mid-NEB wave during Cassini's observations of an expansion event [Li *et al.*, 2006]. Comparing the wave locations in these closely spaced near-IR and thermal-IR maps reveal little evolution during this interval, suggesting that the wave pattern is either very slow or stationary, as confirmed by inspection of the individual $2.16\text{ }\mu\text{m}$ maps used for Figure 3c in Figure S10, which shows no detectable motion during 26–29 January.

A survey of previous detections of mid-NEB waves (Text S2 in the supporting information) reveals an observational bias to periods of previous NEB expansion events, so it is not known whether they are *unique* to periods of expansion. Reported wave numbers have ranged from $N \sim 5\text{--}7$ [Fisher *et al.*, 2016] to $N \sim 12\text{--}13$ [Li *et al.*, 2006], with $2\text{--}4$ K amplitudes at 100 mbar and slow-phase speeds < 5 m/s. The 2016 thermal wave ($N \sim 16\text{--}17$) is therefore the most compact (highest wave number) yet observed. Intriguingly, Orton *et al.* [1994] reported an increase in wave activity between 1988 and 1990 and again in 1993 (compared to their 1978–1993 record), both coinciding with expansion events. The wave pattern characterized by Cassini [Li *et al.*, 2006] also occurred during an expansion. Furthermore, comparison of 890 nm maps acquired by Hubble [Simon *et al.*, 2015] between 2015 and 2016 suggest that the reflectivity wave was not present (or had a lower amplitude) in 2015 (Figure S5). Nevertheless, without a comprehensive time series during nonexpansion periods, any relationship between expansion events and the mid-NEB wave could simply be coincidental.

Besides the quasi-stationary nature of the 2016 wave and the anticorrelation between temperatures and haze reflectivity, the inversions in Figure 2 also show that the wave is confined in both latitude and altitude (not present for $p > 500$ mbar or at 5 mbar). All of these characteristics are similar to those of the 2000–2001 wave, so we follow Li *et al.* [2006] in identifying this as a Rossby wave. Rossby wave confinement occurs due to absorption, wave breaking, and other wave-mean-flow interactions at critical surfaces, where the phase speed c_x approaches the zonal velocity u [Achterberg and Flasar, 1996]. Furthermore, Rossby waves drift westward with respect to the zonal flow, so can only be close to stationary in eastward flow environments [Charney and Drazin, 1961]. Zonal winds estimated from the thermal wind equation in December 2014 by Fletcher *et al.* [2016] (Figure 2f) confirm that the NEB flow is positive (eastward) in the upper troposphere but negative (westward) at both the cloud tops ($p > 200$ mbar) and in the stratosphere ($p < 7$ mbar), with $u \approx c_x \approx 0$ surfaces serving to confine the quasi-stationary wave to the upper troposphere.

Previous studies have suggested multiple origins for these NEB thermal waves, ranging from forcing by phenomena in the deeper interior [Magalhaes *et al.*, 1990; Deming *et al.*, 1997]; forcing by tropospheric meteorology and convective plumes [Andrews *et al.*, 1987]; flow disturbances around vortices [e.g., around White Spot Z, Li *et al.*, 2006]; instabilities associated with the changing sign of the potential vorticity gradient [Achterberg and Flasar, 1996; Read *et al.*, 2006; Rogers *et al.*, 2016]; or the breaking of low-phase-speed Rossby

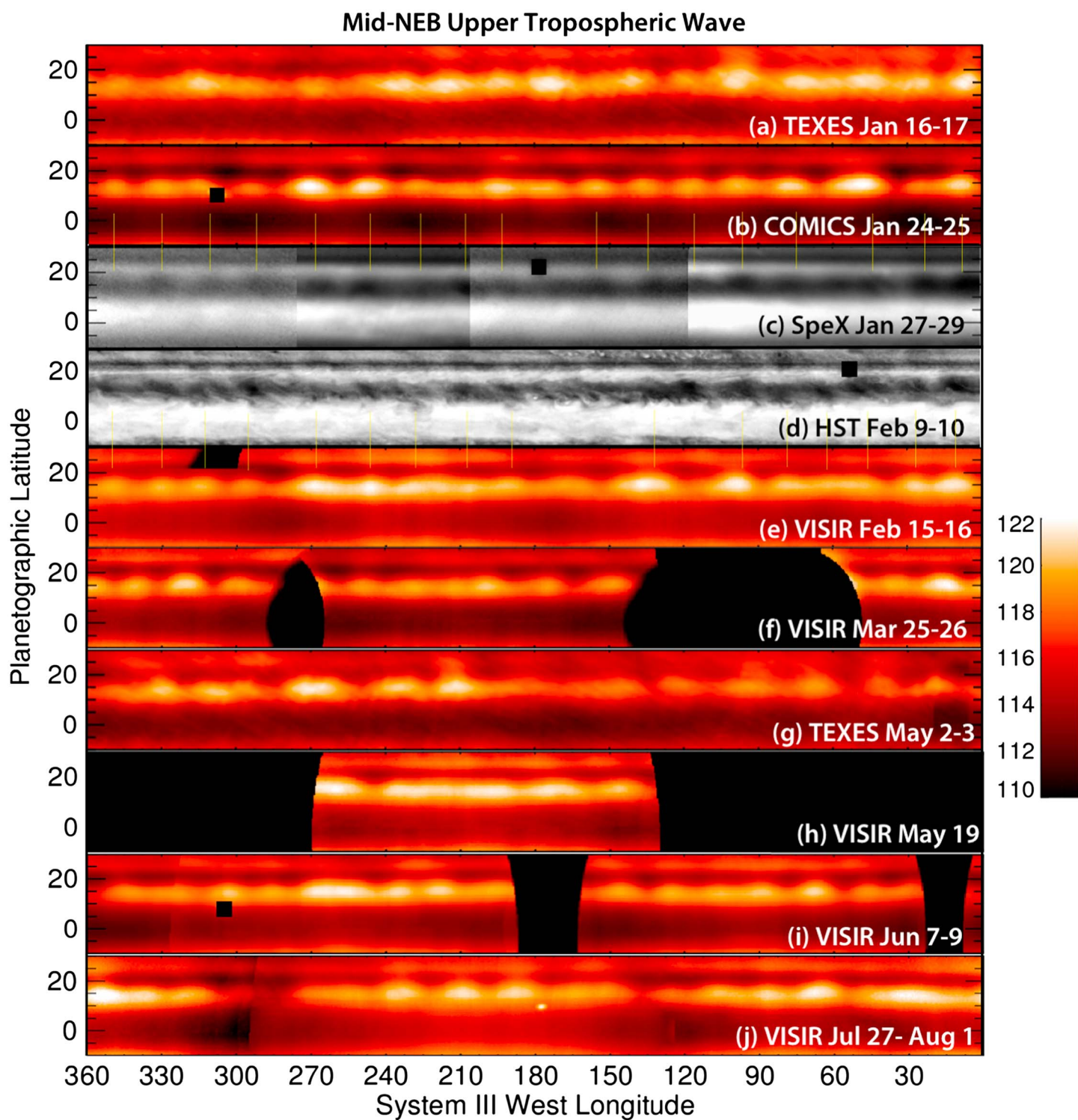


Figure 3. Time series of $17.6\ \mu\text{m}$ brightness temperatures (sensing ~ 150 mbar temperatures) between January and August 2016. IRTF/TEXES maps are an average of the $584\text{--}589\ \text{cm}^{-1}$ spectrum and have a lower spatial resolution than the VLT/VISIR and Subaru/COMICS images. The wave is also shown in tropospheric aerosol reflectivity maps from (c) IRTF/SPeX at $2.16\ \mu\text{m}$ and (d) Hubble WFC3 at $890\ \text{nm}$, with vertical yellow ones showing their correspondence to the thermal wave (see Figure S9). Small black squares denote where Jovian satellites have been removed from Figures 3b–3d and 3i. Spatial coverage gaps are shown as black.

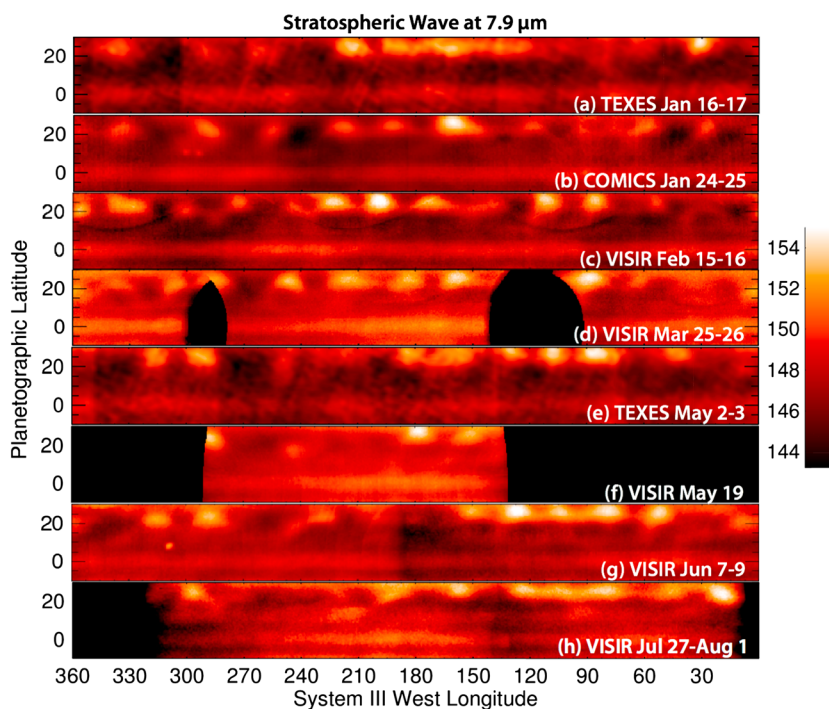


Figure 4. Time series of 7.9 μm brightness temperatures (sensing ~ 5 mbar temperatures) between January and August 2016. IRTF/TEXES maps are an average of the 1243–1252 cm^{-1} spectrum and have a lower spatial resolution than the VLT/VISIR and Subaru/COMICS images. Jovian satellites add artifacts to Figures 4b and 4g near 300°W. Spatial coverage gaps are shown as black.

waves generated by convection in the equatorial region, propagating poleward and depositing energy in regions where u approaches zero [Fisher *et al.*, 2016]. This latter mechanism was based on numerical simulations able to qualitatively reproduce observations [Fisher *et al.*, 2016] and therefore does not require any flow perturbations related to an NEB expansion. A comprehensive time series of wave variability is required to distinguish between these hypotheses.

3.4. Stratospheric NTBs Wave

Filters sensing Jupiter's CH_4 emission at 7.9 μm reveal stratospheric temperatures near the 5 mbar level. The resulting temperature map (Figure 2a) indicates prominent wave activity over the 20–30°N region, covering the NTrZ and North Temperate Belt (NTB), centered on the strong eastward jet at 23.9°N (the NTBs). The mean amplitude of the wave is 7.3 ± 2.2 K at 5 mbar, but with some contrasts up to ~ 11 K (Figure S7).

Figure 4 utilizes brightness temperature maps at 7.9 μm from IRTF, Subaru, and VLT to trace the evolution of this wave over 6 months. Unlike the tropospheric wave, the stratospheric wave exhibits more gaps in the wave train. We observe $N \sim 9$ –13 temperature maxima (Figure S8), depending on the visibility and the longitudinal coverage of each map. Dates in early 2016 with the most complete longitudinal coverage yield horizontal wavelengths of 32,000–38,000 km at 24°N ($N = 11$ –13), making the stratospheric wave distinct from the mid-NEB wave.

Repeated observations in January (TEXES and COMICS) and May (TEXES and VISIR) suggest negligible motion of the wave pattern (Figure 4). However, the motion is irregular and could simply represent the changing visibility of the wave crests with time. Warm spots either side of a gap in the wave train from ~ 200 – 270°W suggest an eastward phase speed of $< 0.1^\circ/\text{d}$ (< 5.5 m/s) in May and June 2016, although we caution the reader that this may not be a unique interpretation. Stratospheric zonal winds estimated from the thermal wind equation (Figure 2f) show that the velocity of the eastward NTBs jet does not vary much with altitude, so this wave has a westward phase speed with respect to the region of eastward u from 20 to 29°N, consistent with a slowly moving Rossby wave in the stratosphere.

Previous reports of stratospheric wave activity are sparse, given the difficulties of observing at 7.9 μm . Orton *et al.* [1991] identified $N = 11$ waves near 22°N from September to December 1988 (during an expansion),

and a stratospheric wave ($N \approx 11$) is evident over the 20–30°N region in the 1–4 mbar temperature maps from Cassini in 2000–2001 [Flasar *et al.*, 2004; Li *et al.*, 2006]. IRTF/TEXES first identified stratospheric wave activity over a limited longitude range to the north and east of WSZ in December 2014, at a time when the northern edge of the NEB was undulating as a precursor to the 2015–2016 expansion [Fletcher *et al.*, 2016]. A more comprehensive time-series of 7.9 μm observations, spanning several expansion events, is required to determine any relationship between these wave phenomena.

4. Conclusions

An Earth-based infrared campaign has characterized Jupiter's atmospheric variability at northern latitudes. The poleward edge of the brown NEB appeared to broaden from 17° to 20°N from November 2015 to March 2016, warming the atmosphere at $p > 500$ mbar and removing white aerosols from the neighboring zone to reveal darker chromophores beneath. This was the eighth such expansion event since 1987 (part of a 3–5 year cycle), but unlike previous events it did not progress to all longitudes, instead remaining limited to a longitude sector $\sim 120^\circ$ west of prominent White Spot Z. After March, the event regressed southward, returning the NEB to normal conditions ahead of Juno's arrival, but leaving a chain of brown barges on the NEBn as evidence of the stalled expansion. The 2016 observations also revealed striking wave patterns, distinct from the $N \approx 12$ equatorial Rossby wave of plumes and hot spots on the NEBs jet (6–9°N, Text S4). Upper tropospheric temperatures in the mid-NEB (13–15°N) exhibited a 2.5 K oscillation at 170 mbar that spanned all longitudes. This wave number $N = 16$ –17 pattern appeared to be quasi-stationary, showed an anticorrelation between temperatures and aerosol reflectivity, and was confined to a region of eastward zonal flow in the upper troposphere so that it was not detected at 5 mbar or at the cloud tops ($p > 500$ mbar). Similar mid-NEB waves with lower wave numbers existed during expansion events in 1988–1989, 1993–1994 [Orton *et al.*, 1994], and 2000–2001 [Rogers *et al.*, 2004; Li *et al.*, 2006], although a comprehensive survey of wave amplitudes over time is required to remove observational bias and to identify any links with NEB expansions. Furthermore, significant stratospheric wave activity was detected at 20–30°N, with wave number $N = 11$ –13, a small-phase speed within an eastward zonal flow, and a mean amplitude of 7.3 ± 2.2 K at 5 mbar. Precursors for this stratospheric wave were identified in December 2014 [Fletcher *et al.*, 2016], and similar stratospheric wave activity was present in 1988 [Orton *et al.*, 1991] and 2001 [Li *et al.*, 2006].

Progress in understanding these wave patterns requires investigations over two very different timescales: (i) shortening the interval between thermal maps to confirm the small-phase velocities of the waves; and (ii) investigation of wave occurrences and amplitudes in the historical record of IR observations and their relation to the cycles of NEB activity. The first may be achieved during the Juno ground-based support campaign in the coming years. The second is required to test any relationship between the NEB expansion cycle and the existence of these waves.

Acknowledgments

All data can be obtained from the primary author (L.N.F., email: leigh.fletcher@leicester.ac.uk) and the relevant observatory archives—full acknowledgements, program IDs and website links are provided in the supporting information. We are extremely grateful to all those participating in the Earth-based support campaign for the Juno mission. Fletcher was supported by a Royal Society Research Fellowship at the University of Leicester. The UK authors were supported by the Science and Technology Facilities Council (STFC). A portion of this work was performed by Orton at the Jet Propulsion Laboratory, California Institute of Technology, under a contract with NASA.

References

- Achterberg, R. K., and F. M. Flasar (1996), Planetary-scale thermal waves in Saturn's upper troposphere, *Icarus*, 119, 350–369, doi:10.1006/icar.1996.0024.
- Adriani, A., et al. (2016), An overview of the Juno JIRAM results from the first perijove pass, Abstract U22A-02 presented at 2016 Fall Meeting, AGU, San Francisco, Calif., 12–16 Dec.
- Allison, M. (1990), Planetary waves in Jupiter's equatorial atmosphere, *Icarus*, 83, 282–307, doi:10.1016/0019-1035(90)90069-L.
- Andrews, D. G., J. R. Holton, and C. B. Leovy (1987), *Middle Atmosphere Dynamics*, Academic Press, New York.
- Arregi, J., J. F. Rojas, A. Sánchez-Lavega, and A. Morgado (2006), Phase dispersion relation of the 5-micron hot spot wave from a long-term study of Jupiter in the visible, *J. Geophys. Res.*, 111, E09010, doi:10.1029/2005JE002653.
- Baines, K., R. Carlson, and L. Kamp (2002), Fresh ammonia ice clouds in Jupiter I. Spectroscopic identification, spatial distribution, and dynamical implications, *Icarus*, 159(1), 74–94.
- Charney, J. G., and P. G. Drazin (1961), Propagation of planetary-scale disturbances from the lower into the upper atmosphere, *J. Geophys. Res.*, 66, 83–109, doi:10.1029/JZ066i001p00083.
- Choi, D. S., A. P. Showman, A. R. Vasavada, and A. A. Simon-Miller (2013), Meteorology of Jupiter's equatorial hot spots and plumes from Cassini, *Icarus*, 223, 832–843, doi:10.1016/j.icarus.2013.02.001.
- Cosentino, R. G., B. Butler, R. J. Sault, R. Morales-Juberías, A. A. Simon, and I. de Pater (2017), Atmospheric waves and dynamics beneath Jupiter's clouds from radio wavelength observations, *Icarus*, 292, 168–181, doi:10.1016/j.icarus.2017.01.006.
- de Pater, I., R. J. Sault, B. Butler, D. DeBoer, and M. H. Wong (2016), Peering through Jupiter's clouds with radio spectral imaging, *Science*, 352, 1198–1201, doi:10.1126/science.aaf2210.
- Deming, D., M. Mumma, F. Espenak, D. Jennings, T. Kostiuk, G. Wiedemann, R. Loewenstein, and J. Piscitelli (1989), A search for p-mode oscillations of Jupiter. Serendipitous observations of nonacoustic thermal wave structure, *Astrophys. J.*, 343, 456–467.
- Deming, D., D. Reuter, D. Jennings, G. Bjoraker, G. McCabe, K. Fast, and G. Wiedemann (1997), Observations and analysis of longitudinal thermal waves on Jupiter, *Icarus*, 126(2), 301–312.
- Fisher, B. M., G. S. Orton, J. Liu, T. Schneider, M. E. Ressler, and W. F. Hoffman (2016), The organization of Jupiter's upper tropospheric temperature structure and its evolution, 1996–1997, *Icarus*, 280, 268–277, doi:10.1016/j.icarus.2016.07.016.

- Flasar, F. M., et al. (2004), An intense stratospheric jet on Jupiter, *Nature*, 427, 132–135.
- Fletcher, L. N., G. S. Orton, P. Yanamandra-Fisher, B. M. Fisher, P. D. Parrish, and P. G. J. Irwin (2009), Retrievals of atmospheric variables on the gas giants from ground-based mid-infrared imaging, *Icarus*, 200, 154–175, doi:10.1016/j.icarus.2008.11.019.
- Fletcher, L. N., G. S. Orton, J. H. Rogers, A. A. Simon-Miller, I. de Pater, M. H. Wong, O. Mousis, P. G. J. Irwin, M. Jacquesson, and P. A. Yanamandra-Fisher (2011), Jovian temperature and cloud variability during the 2009–2010 fade of the South Equatorial Belt, *Icarus*, 213, 564–580, doi:10.1016/j.icarus.2011.03.007.
- Fletcher, L. N., T. K. Greathouse, G. S. Orton, J. A. Sinclair, R. S. Giles, P. G. J. Irwin, and T. Encrenaz (2016), Mid-infrared mapping of Jupiter's temperatures, aerosol opacity and chemical distributions with IRTF/TEXES, *Icarus*, 278, 128–161, doi:10.1016/j.icarus.2016.06.008.
- Fletcher, L. N., G. S. Orton, J. H. Rogers, R. S. Giles, A. V. Payne, P. G. J. Irwin, and M. Vedovato (2017), Moist convection and the 2010–2011 revival of Jupiter's South Equatorial Belt, *Icarus*, 286, 94–117, doi:10.1016/j.icarus.2017.01.001.
- Friedson, A. J. (2005), Water, ammonia, and H₂S mixing ratios in Jupiter's five-micron hot spots: A dynamical model, *Icarus*, 177, 1–17, doi:10.1016/j.icarus.2005.03.004.
- García-Melendo, E., and A. Sánchez-Lavega (2001), A study of the stability of Jovian zonal winds from HST images: 1995–2000, *Icarus*, 152, 316–330, doi:10.1006/icar.2001.6646.
- Hunt, G. E., B. J. Conrath, and J. Pirraglia (1981), Visible and infrared observations of Jovian plumes during the Voyager encounter, *J. Geophys. Res.*, 86, 8777–8781, doi:10.1029/JA086iA10p08777.
- Irwin, P., N. Teanby, R. de Kok, L. Fletcher, C. Howett, C. Tsang, C. Wilson, S. Calcutt, C. Nixon, and P. Parrish (2008), The NEMESIS planetary atmosphere radiative transfer and retrieval tool, *J. Quant. Spectrosc. Radiat. Transfer*, 109(6), 1136–1150.
- Kataza, H., Y. Okamoto, S. Takubo, T. Onaka, S. Sako, K. Nakamura, T. Miyata, and T. Yamashita (2000), COMICS: The cooled mid-infrared camera and spectrometer for the Subaru telescope, in *Optical and IR Telescope Instrumentation and Detectors, Munich, Germany, 27–31 Mar., Society of Photo-Optical Instrumentation Engineers (SPIE) Conf. Ser.*, vol. 4008, edited by M. Iye and A. F. Moorwood, pp. 1144–1152, SPIE, Bellingham, Wash.
- Lacy, J. H., M. J. Richter, T. K. Greathouse, D. T. Jaffe, and Q. Zhu (2002), TEXES: A sensitive high-resolution grating spectrograph for the mid-infrared, *Publ. Astron. Soc. Pac.*, 114, 153–168, doi:10.1086/338730.
- Lagage, P. O., et al. (2004), Successful commissioning of VISIR: The mid-infrared VLT instrument, *Messenger*, 117, 12–16.
- Li, L., A. P. Ingersoll, A. R. Vasavada, A. A. Simon-Miller, R. K. Achterberg, S. P. Ewald, U. A. Dyudina, C. C. Porco, R. A. West, and F. M. Flasar (2006), Waves in Jupiter's atmosphere observed by the Cassini ISS and CIRS instruments, *Icarus*, 185, 416–429, doi:10.1016/j.icarus.2006.08.005.
- Magalhaes, J. A., A. L. Weir, B. J. Conrath, P. J. Gierasch, and S. S. Leroy (1989), Slowly moving thermal features on Jupiter, *Nature*, 337, 444–447, doi:10.1038/337444a0.
- Magalhaes, J. A., A. L. Weir, P. J. Gierasch, B. J. Conrath, and S. S. Leroy (1990), Zonal motion and structure in Jupiter's upper troposphere from Voyager infrared and imaging observations, *Icarus*, 88, 39–72, doi:10.1016/0019-1035(90)90176-A.
- Mousis, O., et al. (2014), Instrumental methods for professional and amateur collaborations in planetary astronomy, *Exp. Astron.*, 38, 91–191, doi:10.1007/s10686-014-9379-0.
- Ortiz, J. L., G. S. Orton, A. J. Friedson, S. T. Stewart, B. M. Fisher, and J. R. Spencer (1998), Evolution and persistence of 5- μ m hot spots at the Galileo probe entry latitude, *J. Geophys. Res.*, 103, 23,051–23,069, doi:10.1029/98JE00696.
- Orton, G. S., et al. (1991), Thermal maps of Jupiter—Spatial organization and time dependence of stratospheric temperatures, 1980 to 1990, *Science*, 252, 537–542.
- Orton, G. S., et al. (1994), Spatial organization and time dependence of Jupiter's tropospheric temperatures, 1980–1993, *Science*, 265, 625–631, doi:10.1126/science.265.5172.625.
- Orton, G. S., C. Hansen, and A. P. Ingersoll (2017), The first close-up images of Jupiter's polar regions: Results from the Juno Mission JunoCam instrument, *Geophys. Res. Lett.*, doi:10.1002/2016GL072443, in press.
- Porco, C. C., et al. (2003), Cassini imaging of Jupiter's atmosphere, satellites, and rings, *Science*, 299, 1541–1547, doi:10.1126/science.1079462.
- Read, P., P. Gierasch, B. Conrath, A. Simon-Miller, T. Fouchet, and Y. Yamazaki (2006), Mapping potential-vorticity dynamics on Jupiter. I: Zonal-mean circulation from Cassini and Voyager 1 data, *Q. J. R. Meteorol. Soc.*, 132, 1577–1603.
- Rogers, J. (1995), *The Giant Planet Jupiter*, Cambridge Univ. Press, Cambridge, U. K.
- Rogers, J., G. Adamoli, G. Hahn, M. Jacquesson, M. Vedovato, and H.-J. Mettig (2013), Jupiter's North Equatorial Belt: An historic change in cyclic behaviour with acceleration of the North Equatorial jet, Abstracts EPSC2013-384 presented at 2013 European Planetary Science Congress, London, U. K., 8–13 Sep.
- Rogers, J. H. (2013), White spot Z: Its history and characteristics, 1997–2013. [Available at http://www.britastro.org/jupiter/2013_14report03.htm.]
- Rogers, J., and G. Adamoli (2015), Jupiter in 2014/15: Final numerical report. [Available at http://www.britastro.org/jupiter/2014_15report12.htm.]
- Rogers, J. H. (2017), Jupiter's North Equatorial Belt and jet: I. Cyclic expansions and planetary waves, *J. Br. Astron. Assoc.*, arXiv:1707.03343 [astro-ph.EP]
- Rogers, J. H., L. N. Fletcher, G. Adamoli, M. Jacquesson, M. Vedovato, and G. S. Orton (2016), A dispersive wave pattern on Jupiter's fastest retrograde jet at 20°S, *Icarus*, 277, 354–369.
- Rogers, J. H. H., T. Akutsu, and G. S. Orton (2004), Jupiter in 2000/2001. Part II: Infrared and ultraviolet wavelengths, *J. Br. Astron. Assoc.*, 114, 313–330.
- Sánchez-Lavega, A., and J. M. Gomez (1996), The South Equatorial Belt of Jupiter, I: Its life cycle, *Icarus*, 121, 1–17, doi:10.1006/icar.1996.0067.
- Showman, A. P., and T. E. Dowling (2000), Nonlinear simulations of Jupiter's 5-micron hot spots, *Science*, 289, 1737–1740, doi:10.1126/science.289.5485.1737.
- Showman, A. P., and A. P. Ingersoll (1998), Interpretation of Galileo probe data and implications for Jupiter's dry downdrafts, *Icarus*, 132, 205–220, doi:10.1006/icar.1998.5898.
- Simon, A. A., M. H. Wong, and G. S. Orton (2015), First results from the Hubble OPAL program: Jupiter in 2015, *Astrophys. J. Lett.*, 812, 55, doi:10.1088/0004-637X/812/1/55.
- Simon-Miller, A. A., D. Banfield, and P. J. Gierasch (2001), Color and the vertical structure in Jupiter's belts, zones, and weather systems, *Icarus*, 154, 459–474, doi:10.1006/icar.2001.6742.
- Tollefson, J., et al. (2017), Changes in Jupiter's zonal wind profile preceding and during the Juno Mission, *Icarus*, 296, 163–178, doi:10.1016/j.icarus.2017.06.007.